

Mixed-state geometric phases of coherent and squeezed spin states

Xin Wang,¹ Jia-Chen Tang,¹ Xu-Yang Hou,¹ Hao Guo,^{1,2,*} and Chih-Chun Chien^{3,†}

¹*School of Physics, Southeast University, Jiulonghu Campus, Nanjing 211189, China*

²*Hefei National Laboratory, Hefei 230088, China*

³*Department of Physics, University of California, Merced, California 95343, USA*

Two mixed-state geometric phases, known as the Uhlmann phase and interferometric phase (IGP), of spin coherent states (CSSs) and spin squeezed states (SSSs) are analyzed. While each phase follows its parallel-transport condition, we also consider the non-adiabatic IGP for arbitrary unitary evolution beyond parallel transport. For the $j = 3/2$ CSS, the Uhlmann phase shows temperature-induced topological phase transitions with jumps. The IGP and non-adiabatic IGP for the $j = 3/2$ CSS also exhibits temperature-induced jumps. In contrast, the Uhlmann phase of the $j = 1$ SSS exhibits smooth behavior without any temperature-induced transition. Interestingly, the parallel-transport condition of the IGP of the $j = 1$ SSS in general does not allow a solution at finite temperature. Instead, the non-adiabatic IGP for the $j = 1$ SSS has a solution showing smooth behavior as the squeezing parameter and temperature change. We also briefly discuss possible experimental implications and simulations.

I. INTRODUCTION

Geometric phases have been a key concept in topological properties of quantum systems [1, 2]. The Berry phase arises when a quantum system undergoes adiabatic cyclic evolution in the context of pure quantum states and has been fundamental in studying topological insulators and superconductors, where the Berry curvature characterizes the underlying topological features [3–16]. However, quantum systems are often in mixed states due to finite temperatures or non-equilibrium conditions, which call for generalizations of the Berry phase to mixed quantum states. A mathematically rigorous approach is the Uhlmann phase [17–20] for mixed states. Like the Berry phase, the Uhlmann phase is obtained from parallel transport in a cyclic process, and the Uhlmann-Berry correspondence shows that the Uhlmann phase in the low-temperature limit generally agrees with the Berry phase of the ground state [21]. However, the Uhlmann bundle is trivial [22], which limits its applicability to defining other quantized topological indices. Nevertheless, the Uhlmann phase of bosonic and fermionic coherent states have been studied [21], in addition to that of two-level and spin- j systems [23–25]. With a suitable generalization, the Uhlmann phase of dynamic systems has also been studied [26].

Another approach called the interferometric geometric phase (IGP) for mixed states has been proposed [27] and further analyzed [28–32], extending the geometric phase concept via an analogy of the optical Mach-Zehnder interferometer [33]. This IGP has been experimentally observed using nuclear magnetic resonance and polarized neutrons [33–36]. Unlike the Uhlmann phase, the IGP does not require the evolution of the system to be cyclic [27]. In some cases, it can be shown that the IGP

is the argument of the weighted sum of the Berry-phase factors of the constituent states [27].

Ref. [37] presents a comparison between the Uhlmann phase and IGP to contrast their differences. The Uhlmann phase, for instance, requires the ancillary system modeling environmental effects to be manipulated according to the change of the system and can exhibit finite-temperature topological phase transitions with quantized jumps in two-level systems. In contrast, the IGP does not exhibit such transitions at finite temperatures for general two-level systems. Recent studies have demonstrated that the IGP remains intact as temperature varies for the Kitaev chain [38], in contrast to the discrete jumps seen in the Uhlmann phase [23]. Nevertheless, quantized jumps of the IGP as temperature increases can occur in three-level or higher-dimensional systems [37]. Interestingly, these generalizations of the mixed-state geometric phases provide further insights into topological quantum phase transitions (TQPTs) and dynamical quantum phase transitions (DQPTs) [39].

Meanwhile, spin systems have served as paradigms in various physics branches, ranging from quantum mechanics [40] to statistical physics [41] to spintronic devices [42]. Two types of spin states have received particular attention: The coherent spin states (CSSs) are minimal uncertainty states of collective angular momentum. The CSS is the building block for the path-integral description of many-body spin systems [43] and serves as a classical approximation of quantum spin systems, thereby establishing the standard quantum limit (SQL) for measurements [44–47]. However, surpassing the SQL is critical for advancing quantum metrology and quantum information technologies. Spin squeezing [48–50] allows for a reduction of the variance of one spin component at the expense of increasing that of another orthogonal direction, resulting in the squeezed spin states (SSSs). The SSSs enable precision measurements beyond the SQL and approach the Heisenberg limit with potential applications in, for example, atomic clocks [51, 52]. Significant improvements in precision measurement using spin squeez-

* guohao.ph@seu.edu.cn

† cchien5@ucmerced.edu

ing have also been made in atomic Bose-Einstein condensates (BECs) [53, 54]. These developments not only highlight the metrological advantage of the SSS but also open possible avenues for generating quantum entanglement in many-body systems, fostering further advancement in quantum information processing [55].

Complementing the progress in surpassing the SQL through spin squeezing, here we set to investigate the geometric phases of the CSS and SSS at finite temperatures and search for topological phases or transitions. The possibility of finding different mixed-state geometric phases according to different evolution conditions already demonstrates rich physics in the underlying topology of finite-temperature systems. While the geometric phase of the ground-state CSS has been analyzed [56, 57], here we explicitly calculate the Uhlmann phase and the IGP for selected CSS and SSS at finite temperatures. We found that for the $j = 3/2$ CSS, both Uhlmann phase and IGP demonstrate temperature-dependent topological or geometric phase transitions with quantized jumps. The jumps survive after generalizing the IGP to the non-adiabatic IGP for the CSS. In contrast, the $j = 1$ SSS has a smoothly-varying Uhlmann phase as temperature increases, so there is no topological phase transition. More interestingly, the parallel-transport condition of the $j = 1$ SSS cannot be satisfied at finite temperatures in general, leaving a construction of the IGP impractical. We therefore analyze the non-adiabatic IGP for the $j = 1$ SSS to circumvent the obstacle but found no discrete jump in the geometric contribution of the phase at finite temperature.

The rest of the paper is organized as follows. Sec. II provides a self-contained theoretical background, covering the CSS, SSS, Uhlmann phase, and the adiabatic and non-adiabatic IGPs. Sec. III and Sec. IV present our systematic investigations of the mixed-state geometric phases for selected cases of the CSS and SSS, respectively. Section V discusses possible experimental and theoretical implications of our findings. Finally, Sec. VI concludes our work.

II. THEORETICAL BACKGROUND

We begin with a brief overview of the CSS and SSS as well as a short review of the Uhlmann phase and interferometric geometric phase (IGP) of mixed states. Additionally, we will generalize the concept of IGP to allow arbitrary unitary evolution. For simplicity, we set $c = \hbar = k_B = 1$ throughout the paper.

A. Overview of CSS

The spin operators satisfy the algebra [40]

$$[J_z, J_+] = J_+, \quad [J_z, J_-] = -J_-, \quad [J_+, J_-] = 2J_z. \quad (1)$$

The eigenstates of J^2 and J_z are $|jm\rangle$, $-j \leq m \leq j$. Moreover, $J_\pm |jm\rangle = \sqrt{(j \mp m)(j \pm m + 1)} |jm \pm 1\rangle$ and $J_z |jm\rangle = m |jm\rangle$. The CSS is defined as [58, 59]

$$|\xi\rangle := e^{\xi J_+ - \bar{\xi} J_-} |j, -j\rangle, \quad (2)$$

where $\xi \in \mathbb{C}$ is a complex number.

Using the Baker-Campbell-Hausdorff disentangling formula [58], the CSS can also be expressed as

$$\begin{aligned} |\xi\rangle &= e^{\zeta J_+} e^{\ln(1+|\zeta|^2) J_z} e^{-\bar{\zeta} J_-} |j, -j\rangle \\ &= \frac{1}{(1+|\zeta|^2)^j} e^{\zeta J_+} |j, -j\rangle \equiv |\zeta\rangle \end{aligned} \quad (3)$$

with $\zeta = \zeta(\xi) = \frac{\xi \tan |\xi|}{|\xi|}$. After defining $D(\xi) \equiv D(\zeta) = e^{\xi J_+ - \bar{\xi} J_-}$, the CSS corresponds to the ground state of the translated Hamiltonian $\hat{H}(\xi) \equiv \hat{H}(\zeta) = D(\zeta) \hat{H} D^\dagger(\zeta)$. Here $\hat{H} = \omega_0 J_z$, and ω_0 is the Larmor frequency. The associated excited states are obtained in a similar manner: $|jm, \xi\rangle = |jm, \zeta\rangle = D(\zeta) |jm\rangle$, $-j \leq m \leq j$. By parameterizing ξ as $\xi = e^{-i\phi} \frac{\theta}{2}$, we have $\zeta = e^{-i\phi} \tan \frac{\theta}{2}$. If the parameter ranges are chosen as $0 \leq \phi \leq 2\pi$, $0 \leq \theta \leq \pi$, then ζ spans the entire complex plane. Consequently, we will use ζ as the control parameter. The map $(\theta, \phi) \rightarrow \zeta$ projects the unit sphere onto the entire complex plane. Actually, the CSSs are closely related to the eigenstates of the corresponding spin- j system with the Hamiltonian $H = \omega_0 \hat{\mathbf{B}} \cdot \mathbf{J}$, where $\hat{\mathbf{B}}$ is the unit vector pointing along the direction of an external magnetic field [43].

B. Overview of SSS

A spin- j system can be regarded as a composite system consisting of $2j$ spin- $\frac{1}{2}$ objects. The angular momentum operators for the collection of spin- $\frac{1}{2}$ objects are given by

$$J_\alpha = \frac{1}{2} \sum_{l=1}^N \sigma_{l\alpha}, \quad \alpha = x, y, z, \quad (4)$$

where $\sigma_{l\alpha}$ is the Pauli matrix for the l -th object. Here we consider the spin-squeezed states (SSS) generated by the one-axis twisting Hamiltonian [49, 60]

$$H_{\text{OAT}} = \eta J_x^2 = \frac{\eta}{4} \sum_{k,l=1}^N \sigma_{kx} \sigma_{lx}, \quad (5)$$

which is a nonlinear operator with the coupling constant η involving all pairwise interactions. This indicates the presence of pairwise correlations in the spin-squeezed states generated by the Hamiltonian. Choosing the initial state as $|j, -j\rangle = |1\rangle^{\otimes N}$, where $|1\rangle = |j = 1/2, j_z = 1/2\rangle$, the SSS at time t is formally written as:

$$|\Psi(t)\rangle = \exp(-i\Theta J_x^2/2) |1\rangle^{\otimes N}, \quad (6)$$

where $\Theta = 2\eta t$.

We can generalize this concept of spin-squeezed states by acting the operator $\exp(-i\Theta J_x^2/2)$ on $|jm\rangle$:

$$|jm, \Theta\rangle = \exp(-i\Theta J_x^2/2) |jm\rangle. \quad (7)$$

By defining

$$S(\Theta) = e^{-i\Theta J_x^2/2}, \quad (8)$$

then $|jm, \Theta\rangle$ is an eigenstate of the Hamiltonian

$$H(\Theta) = S(\Theta)\omega_0 J_z S^\dagger(\Theta). \quad (9)$$

C. Uhlmann phase

A mathematically rigorous approach for generalizing the Berry phase from pure states to mixed states is the Uhlmann phase [17] through purification of density matrices, which can be described by the underlying fiber-bundle structure [61]. An operator W is said to purify the density matrix ρ if $\rho = WW^\dagger$. Conversely, the purification W can be uniquely decomposed as $W = \sqrt{\rho}\mathcal{U}$ if ρ is full-rank (i.e., $\text{rank}(\rho) = N$ for a system with a N -dimensional Hilbert space). Here the unitary operator \mathcal{U} is referred to as the phase factor of mixed states, representing a generalization of the $U(1)$ phase factor associated with pure states.

We consider a system depending on a set of parameters $\mathbf{R} = (R_1, R_2, \dots, R_k)^T \in M$, where M is the parameter manifold. When ρ evolves along a smooth curve $C(t) := \mathbf{R}(t)$ in M , the purification of the density matrix also continuously evolves along an induced curve $\gamma(t) := W(t) = \sqrt{\rho(\mathbf{R}(t))}\mathcal{U}(\mathbf{R}(t))$. If the length of γ , defined as $L(\gamma) = \int_\gamma \sqrt{\text{Tr}(\dot{W}\dot{W}^\dagger)} dt$, is minimized, W is said to undergo a parallel-transport process. Therefore, $\gamma(t)$ is the horizontal lift of $\rho(t) \equiv \rho(\mathbf{R}(t))$. It can be shown that the Uhlmann parallel-transport condition is given by [62]

$$\dot{W}W^\dagger = W\dot{W}^\dagger. \quad (10)$$

This condition maximally ensures the ‘‘parallelity’’ between purification of adjacent states.

When ρ experiences a cyclic evolution over a duration τ , such that $\rho(0) = \rho(\tau)$, the evolution of its purification may not necessarily return to its initial value. Specifically, the initial and final phase factors of a Uhlmann process are related by

$$\mathcal{U}(\tau) = \mathcal{P}e^{-\oint_C A_U} \mathcal{U}(0), \quad (11)$$

where \mathcal{P} is the path-ordering operator and

$$A_U = - \sum_{mn} |m\rangle \frac{\langle m | [d\sqrt{\rho}, \sqrt{\rho}] | n \rangle}{\lambda_m + \lambda_n} \langle n| \quad (12)$$

is the Uhlmann connection. Here λ_n , $|n\rangle$ represent the eigenvalues and eigenstates of ρ , respectively. Notably,

the parallelity lacks transitivity [39] even during parallel transport. Hence, the operator $\mathcal{P}e^{-\oint_C A_U}$ associated with the Uhlmann holonomy quantifies a measure of the loss of parallelity. The following Uhlmann phase then reflects the topological change of the Uhlmann holonomy.

$$\theta_U(C) = \arg \text{Tr}(W^\dagger(0)W(\tau)) = \arg \text{Tr}[\rho(0)\mathcal{P}e^{-\oint_C A_U}]. \quad (13)$$

D. Interferometric geometric phase

There is another approach for constructing a geometric phase for mixed states. Inspired by optical processes in the Mach-Zehnder interferometer, Ref. [27] assigned a phase to a mixed quantum state represented by the density matrix ρ undergoing a unitary evolution $U(t)$. Explicitly, if a system evolves according to $\rho(t) = U(t)\rho(0)U^\dagger(t)$, it gives rise to a total phase

$$\theta_T(t) = \arg \text{Tr}[\rho(0)U(t)]. \quad (14)$$

Notably, the transformation from $\rho(t)$ to $\rho(t+dt)$ is $\rho(t+dt) = U(t+dt)\rho(0)U^\dagger(t+dt) = U(t+dt)U^\dagger(t)\rho(t)U(t)U^\dagger(t+dt)$. Thus, by definition, the relative phase between the mixed states at t and $t+dt$ is $\theta_T(t) = \arg \text{Tr}[\rho(t)U(t+dt)U^\dagger(t)]$. In this framework [27], a parallel-transport condition of $U(t)$ is proposed as follows. $\rho(t+dt)$ is required to be instantaneously ‘‘in phase’’ with $\rho(t)$, which means $\arg \text{Tr}[\rho(t)U(t+dt)U^\dagger(t)] = 0$. In the differential form, the condition yields

$$\text{Tr}[\rho(t)\dot{U}(t)U^\dagger(t)] = \text{Tr}[\rho(0)U^\dagger(t)\dot{U}(t)] = 0. \quad (15)$$

To specify parallel-transport by the evolution according to $U(t)$ more accurately, the condition (15) has been strengthened as [27]

$$\langle n(t) | \dot{U}(t) U^\dagger(t) | n(t) \rangle = 0, \quad n = 0, 1, 2, \dots, \quad (16)$$

where $|n(t)\rangle$ is the n th eigen-vector of $\rho(t)$. We emphasize that the above parallel-transport condition is distinct from the Uhlmann parallel-transport condition (10) which depends explicitly on the choice of the $U(N)$ phase factor \mathcal{U} .

Under the parallel-transport condition, the total phase accumulated during the evolution is the geometric phase referred to as the IGP:

$$\theta_G(t) = \theta_T(t) = \arg \text{Tr}[\rho(0)U(t)]. \quad (17)$$

This is because there is no accumulation of the dynamic phase during parallel transport, which can be understood by noting that if $U(t)$ represents a dynamic evolution process according to $i\dot{U} = HU$, the parallel-transport condition (15) guarantees

$$\theta_D(t) = - \int_0^t dt' \text{Tr}[\rho(t')H(t')]$$

$$= -i \int_0^t dt' \text{Tr} \left[\rho(t') \dot{U}(t') U^\dagger(t') \right] = 0. \quad (18)$$

As a consequence, the total phase contains only the geometric contribution from the IGP.

In certain situations, it may be difficult for unitary evolutions to fully satisfy the parallel-transport condition (15). Nevertheless, the above discussion can be extended to general unitary evolution beyond parallel transport, which results in non-adiabatic phases [63]. For pure states, a similar formalism is known as the quantum kinematic approach to the geometric phase [64]. Recently, a similar non-adiabatic geometric phase for mixed states has been discussed in Ref. [65]. We follow those ideas and define the non-adiabatic IGP for any unitary process by subtracting the non-adiabatic generalization of the dynamic phase from the total phase. Explicitly,

$$\theta'_G(t) = \theta_T(t) - \theta_{\text{NG}}(t). \quad (19)$$

Here

$$\theta_{\text{NG}}(t) = -i \int_0^t dt' \text{Tr} \left[\rho(t') \dot{U}(t') U^\dagger(t') \right] \quad (20)$$

is considered as a non-geometric phase because if $U(t)$ represents a dynamic evolution, $\theta_{\text{NG}}(t)$ reduces to the dynamic phase. Moreover, if $U(t)$ satisfies the parallel-transport condition, $\theta_{\text{NG}}(t) = 0$, and the total phase equals to the geometric phase given by the IGP.

E. Difference between the two geometrical phases

We emphasize that the two aforementioned geometric phases for mixed states are physically and mathematically distinct. Although the theory of IGP can also be formulated equivalently using a purification formalism of density matrices [27], any phase factor \mathcal{U} is ruled out in the derivation. Specifically, only the trivial decomposition $W = \sqrt{\rho}$ is permissible for the IGP because otherwise the condition (15) would be violated.

In contrast, the generation of the Uhlmann phase inherently relies on the phase factor \mathcal{U} according to the underlying fiber-bundle structure. All purifications of a given density matrix ρ thus span a $U(N)$ fiber space. Consequently, the Uhlmann phase is naturally and directly connected to the topological properties of the $U(N)$ principal bundle, a feature absent in the IGP. Explicitly, the Uhlmann phase corresponds to the Uhlmann holonomy of the Uhlmann bundle of density matrices, similar to the Berry phase revealing the Berry holonomy of the fiber bundle of pure states [61]. Moreover, the Uhlmann phase requires a cyclic process but is guaranteed to be gauge invariant [27, 37] while the IGP and its generalization do not impose those constraints. In the following, we will compare the differences between the Uhlmann phase and IGP through specific examples of the CSS and SSS.

III. GEOMETRICAL PHASES OF CSS

A. The Uhlmann phase

To evaluate the Uhlmann phase, we consider a loop in the complex ζ plain: $C(t) \equiv \zeta(t)$, $0 \leq t \leq \tau$ with $\zeta(0) = \zeta(\tau)$. The continuous transformation $D(\zeta(t))$ of a CSS at temperature T induces a corresponding loop $\gamma(t) := \rho(\zeta(t))$ in the manifold of density matrices, where

$$\rho(\zeta) = \frac{1}{Z} e^{-\beta \hat{H}(\zeta)} = \frac{1}{Z} D(\zeta) e^{-\beta \hat{H}} D^\dagger(\zeta). \quad (21)$$

Here $\beta = 1/(k_B T)$. Since $D(\zeta)$ is unitary, the eigenvalues of the Hamiltonian remain invariant under $D(\zeta)$. As a result, the partition function is a constant: $Z = \sum_{m=-j}^j e^{-m\beta\omega_0} = \frac{\sinh[(j+\frac{1}{2})\beta\omega_0]}{\sinh(\frac{\beta\omega_0}{2})}$.

According to Eq. (12), the Uhlmann connection of the CSS is given by

$$\begin{aligned} A_U &= - \sum_{n \neq m} \frac{(\sqrt{\lambda_n} - \sqrt{\lambda_m})^2}{\lambda_n + \lambda_m} |jn, \zeta\rangle \langle jn, \zeta| d|jm, \zeta\rangle \langle jm, \zeta| \\ &= - \sum_{n \neq m} \chi_{nm} D(\zeta) |jn\rangle \langle jn| D^\dagger(\zeta) dD(\zeta) |jm\rangle \langle jm| D^\dagger(\zeta), \end{aligned} \quad (22)$$

where $\lambda_m = \frac{1}{Z} e^{-m\beta\omega_0}$ is the m th eigenvalue of the density matrix, and $\chi_{nm} = \frac{(e^{-\frac{n}{2}\beta\omega_0} - e^{-\frac{m}{2}\beta\omega_0})^2}{e^{-n\beta\omega_0} + e^{-m\beta\omega_0}}$. By applying Eq. (3), we further get

$$D^\dagger(\zeta) dD(\zeta) = \frac{J_+ d\zeta - J_- d\bar{\zeta}}{1 + |\zeta|^2} + J_z \frac{\zeta d\bar{\zeta} - \bar{\zeta} d\zeta}{1 + |\zeta|^2}. \quad (23)$$

Accordingly, the Uhlmann connection becomes

$$\begin{aligned} A_U &= - \sum_{n \neq m} \frac{\chi_{nm}}{1 + |\zeta|^2} \times \\ &D(\zeta) |jn\rangle \langle jn| (J_+ d\zeta - J_- d\bar{\zeta}) |jm\rangle \langle jm| D^\dagger(\zeta) \\ &= - \frac{\chi}{(1 + |\zeta|^2)^2} [J_+ (d\zeta + \zeta^2 d\bar{\zeta}) - J_- (d\bar{\zeta} + \bar{\zeta}^2 d\zeta) \\ &\quad + 2J_z (\zeta d\bar{\zeta} - \bar{\zeta} d\zeta)], \end{aligned} \quad (24)$$

where $\chi \equiv \chi_{n+1,n} = \chi_{n-1,n} = 1 - \text{sech} \frac{\beta\omega_0}{2}$. The $n = m$ terms have been included to simplify the expression since $\chi_{nn} = 0$ gives no contributions.

Next, noting that $d\zeta = -i d\theta e^{-i\phi} \sec^2 \frac{\theta}{2}$, we obtain the final expression of A_U :

$$\begin{aligned} A_U &= i\chi [(J_x \cos \phi + J_y \sin \phi) \cos \theta - J_z \sin \theta] \sin \theta d\phi \\ &\quad + i\chi (J_x \sin \phi - J_y \cos \phi) d\theta. \end{aligned} \quad (25)$$

Using Eq. (25), the Uhlmann phase generated in a cyclic process can be evaluated. The A_U of the CSS only differs by a minus sign from that of the spin- j system discussed in Ref. [66]. Therefore, their Uhlmann phases only differ

by a minus sign. As explained in Sec. II, this is because the CSS is related to the spin- j system with a particular Hamiltonian. Since the cases with $j = \frac{1}{2}$ and 1 of the corresponding spin- j systems have already been studied in Ref. [66], we will focus here on the $j = \frac{3}{2}$ CSS. In Appendix A, we show that (I) the Uhlmann phase reduces to the Berry phase associated with the ground state as $T \rightarrow 0$, thereby confirming the correspondence explained in Ref. [21], and (II) the $T \rightarrow 0$ expressions of the CSSs agree with those of Ref. [56] for pure states.

To explicitly show the properties of the Uhlmann phase of a $j = \frac{3}{2}$ CSS, we choose the case evolving along the equator ($\theta = \frac{\pi}{2}$) in the parameter space. In this case, the Uhlmann connection reduces to $A_U = -i\chi J_z d\phi$. The spin operators are

$$\begin{aligned} J_x &= \begin{pmatrix} 0 & \frac{\sqrt{3}}{2} & 0 & 0 \\ \frac{\sqrt{3}}{2} & 0 & 1 & 0 \\ 0 & 1 & 0 & \frac{\sqrt{3}}{2} \\ 0 & 0 & \frac{\sqrt{3}}{2} & 0 \end{pmatrix}, \\ J_y &= \begin{pmatrix} 0 & \frac{i\sqrt{3}}{2} & 0 & 0 \\ -\frac{i\sqrt{3}}{2} & 0 & i & 0 \\ 0 & -i & 0 & \frac{i\sqrt{3}}{2} \\ 0 & 0 & -\frac{i\sqrt{3}}{2} & 0 \end{pmatrix}, \\ J_z &= \begin{pmatrix} -\frac{3}{2} & 0 & 0 & 0 \\ 0 & -\frac{1}{2} & 0 & 0 \\ 0 & 0 & \frac{1}{2} & 0 \\ 0 & 0 & 0 & \frac{3}{2} \end{pmatrix}. \end{aligned} \quad (26)$$

We also assume that the evolution starts from $\phi = 0$, so the initial density matrix is given by $\rho(0) = \frac{1}{Z} e^{\frac{i\pi}{2} J_y} e^{-\beta\omega_0 J_z} e^{-\frac{i\pi}{2} J_y}$ according to Eq. (21). A straightforward evaluation shows that the Uhlmann phase generated in this process is

$$\theta_U = \arg \text{Tr} \left[\frac{1}{Z} e^{\beta\omega_0 J_x} \mathcal{P} e^{i\chi \oint_{\gamma} J_z d\phi} \right], \quad (27)$$

where we have used the fact $e^{i\theta J_y} J_z e^{-i\theta J_y} = -J_x \sin \theta + J_z \cos \theta$.

We plot θ_U as a function of T in Figure 1. In the low temperature limit, $\theta_U = \pi$, which indicates that the topological properties of the system change after a cyclic evolution along the equator. More specifically, the final purification (in terms of the fiber in the bundle language) is ‘‘antiparallel’’ to the initial purification. As temperature increases and crosses the first critical temperature $T_c^1 \approx 0.321\omega_0$, the value of θ_U suddenly drops to 0, implying that a topological change occurs in the evolution along the equator on the parameter space. The final purification now becomes ‘‘parallel’’ to the initial purification. As temperature continues to rise, subsequent topological transitions occur at $T_c^2 \approx 0.376\omega_0$ and $T_c^3 \approx 0.493\omega_0$. In the high temperature limit, θ_U remains zero, meaning the associated Uhlmann holonomy is topologically trivial. This is reasonable since

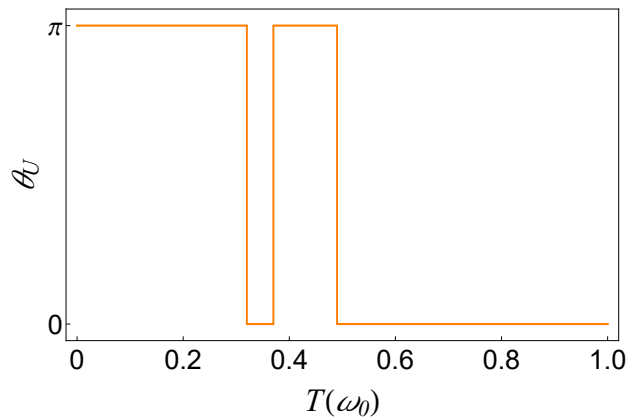


Figure 1. Uhlmann phase θ_U versus temperature for the CSS with $j = \frac{3}{2}$ along $\theta = \frac{\pi}{2}$.

$\lim_{T \rightarrow 0} \rho = \frac{1}{4} \mathbf{1}_{4 \times 4}$. Therefore, the evolution loop $\rho(t)$ essentially becomes a single point with its horizontal lift $W(t)$ also reduced to a single point [66]. Hence, there is no difference between the initial and final fibers anymore. We mention that bosonic and fermionic coherent states at finite temperatures, in contrast, have been shown to have smooth behavior of the Uhlmann phase without any jumps [21].

B. The interferometric geometric phase

Here we first evaluate the IGP for the CSS following unitary evolution that satisfies the parallel-transport condition (15). A natural candidate is the transformation that generates the CSS, as shown in Eq. (21). This yields

$$\rho(t) \equiv \rho(\zeta(t)) = D(\zeta(t))\rho(0)D^\dagger(\zeta(t)), \quad (28)$$

where $\rho(0) = \frac{1}{Z} e^{-\beta\hat{H}}$. Initially, we set $\zeta(0) = 0$, implying $\theta(0) = 0$. Using Eq. (23), the parallel-transport condition (15) can be satisfied by requiring

$$\begin{aligned} & \text{Tr} [\rho(0) D^\dagger(\zeta) dD(\zeta)] \\ &= \sum_m \frac{e^{-m\beta\omega_0}}{Z} \langle jm | \frac{J_+ d\zeta - J_- d\bar{\zeta} + J_z (\zeta d\bar{\zeta} - \bar{\zeta} d\zeta)}{1 + |\zeta|^2} | jm \rangle \\ &= \frac{2i}{Z(1 + |\zeta|^2)} \sum_{m=-j}^j m e^{-m\beta\omega_0} \left(\tan^2 \frac{\theta}{2} d\phi \right) \\ &= 0. \end{aligned} \quad (29)$$

A possible choice is $\tan^2 \frac{\theta}{2} d\phi = 0$, which implies either $\theta = 0$ or $d\phi = 0$. The former leads to $\zeta = 0$, indicating that $D(\zeta) = 1$, which is a trivial evolution. Therefore, we choose the latter and set ϕ to be constant. This represents a longitude on the unit-sphere parameter space shown by the big circle in Figure 2.

To explicitly show the properties of the IGP along a path of fixed ϕ , we set $j = \frac{3}{2}$ as the case of the Uhlmann

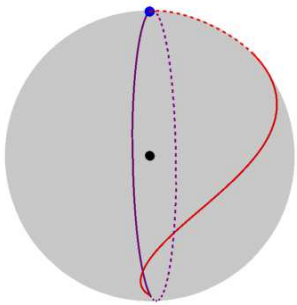


Figure 2. The great circle represents a longitude with constant ϕ on the unit-sphere parameter space, which satisfies the parallel-transport condition (29). In contrast, the twisting curve denotes a simple evolutionary path with $\theta = \phi$, which does not fulfill the parallel-transport condition. Both paths start from the north pole, depicted by the top blue point.

phase and found

$$\begin{aligned} \theta_G(t) &= \arg \text{Tr}[\rho(0)D(t)] \\ &= \arg \text{Tr}\left[\frac{1}{Z}e^{-\beta\omega_0 J_z} e^{\zeta(t)J_+} e^{\ln(1+|\zeta(t)|^2)J_z} e^{-\bar{\zeta}(t)J_-}\right] \\ &= \arg \left[-2e^{\beta\omega_0} \tan^2\left(\frac{\theta(t)}{2}\right) + e^{2\beta\omega_0} + 1 \right]. \quad (30) \end{aligned}$$

Interestingly, the result is independent of ϕ . To visualize the behavior of the IGP, we introduce $\theta_f \equiv \theta(t_{\text{final}})$ as the final value of θ at the end of evolution by $D(t)$. In the top panel of Figure 3, we present the contour plot of the IGP as a function of T and θ_f for $j = \frac{3}{2}$. One observes that when $\theta_f \in (\frac{\pi}{2}, \frac{3\pi}{2})$, the value of the IGP undergoes a sudden jump from 0 to π as the system crosses a critical temperature T_c . This means that $\rho(t_{\text{final}}, T_c^-)$ is in phase with $\rho(0, T_c^-)$, whereas $\rho(t_{\text{final}}, T_c^+)$ is out of phase with $\rho(0, T_c^+)$.

In the bottom panel of Figure 3, we choose a special case with $\theta_f = \frac{3}{4}\pi$ to show the discontinuity of the IGP at $T_c = 0.408\omega_0$. Similar to the case of the Uhlmann phase, this can be recognized as a geometric phase transition induced by temperature. The only difference is that, in general, the IGP is not directly related to the topological properties of the system. Furthermore, finite-temperature geometric phase transitions of the IGP seem to be less common than those of the Uhlmann phase. For a two-level Hermitian quantum system, a finite change in temperature in general does not induce any jump of the IGP [37, 67]. For a three-level system, a careful design of the evolution process can make it happen [37]. Our results of the CSS thus illustrate additional transitions of the IGP and show that the CSS is suitable for studying interesting properties of mixed-state geometric phases.

The above studies can also be extended to generic unitary evolutions which do not necessarily satisfy the parallel-transport condition (29). As previously noted, the non-adiabatic IGP is generated during these evolu-

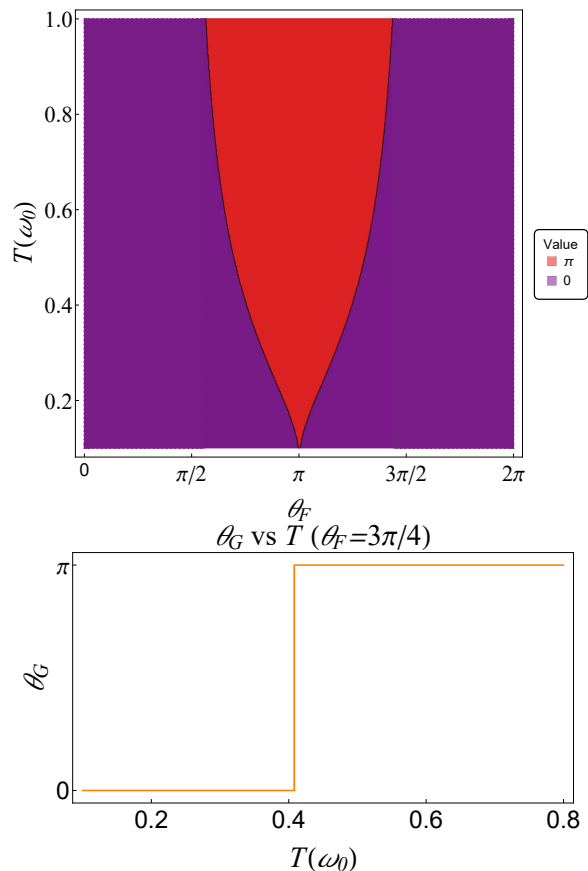


Figure 3. (Top panel) Contour plot of the IGP θ_G versus temperature T and θ_f for $j = \frac{3}{2}$. The geometric phase transitions when $\theta_f \in (\frac{\pi}{2}, \frac{3\pi}{2})$ are indicated by the boundaries separating the two values of θ_G . (Bottom panel) θ_G versus temperature T for the case with $\theta_f = \frac{3\pi}{4}$.

tions according to Eq. (19):

$$\theta'_G(t) = \arg \text{Tr}[\rho(0)D(t)] + i \int_0^t \text{Tr} \left[\rho(0)D^\dagger(t')\dot{D}(t') \right] dt'. \quad (31)$$

The evolution is characterized by a trajectory $\theta = f(\phi)$ or, conversely, $\phi = g(\theta)$ in the parameter space. To contrast with the IGP, we focus on evolution during which θ'_G exhibits finite jumps. Specifically, a simple evolutionary curve C defined by $\theta(t) = \phi(t)$ with $\phi \in [0, \pi]$ is selected, as shown by the twisting curve in Fig. 2. This curve starts at $\theta = 0$ when $t = 0$ and ends at any point (θ_f, ϕ_f) along the path, where $\theta_f \equiv \theta(t_{\text{final}})$ and $\phi_f \equiv \phi(t_{\text{final}})$. In the top panel of Figure 4, we present the contour plot of θ'_G as a function of T and ϕ_f for the $j = \frac{3}{2}$ CSS. Although θ'_G is not quantized, its value still undergoes quantized jumps. To better illustrate those jumps, we plot θ'_G vs T with $\theta_f = \frac{3\pi}{4}$ and θ'_G vs θ_f with $T = 0.6\omega_0$, respectively, in the bottom panels of Fig. 4.

Interestingly, the critical temperature $T_c = 0.408\omega_0$ with a π -jump when $\theta_f = \frac{3\pi}{4}$ is identical to that observed along the path with constant ϕ which respects

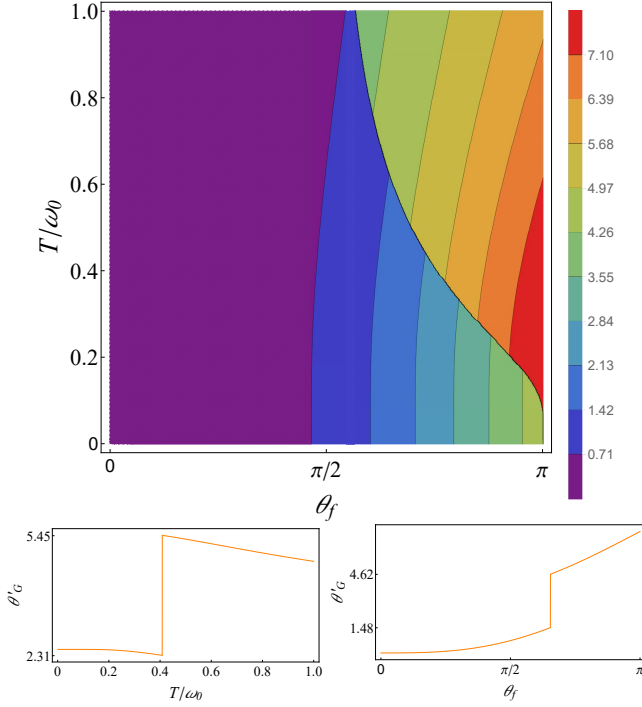


Figure 4. (Top panel) The non-adiabatic IGP θ'_G as a function of T and ϕ_f , where $\theta_f = \phi_f$ corresponding to $\theta_f \in [0, \frac{3\pi}{4}]$. The black curve indicates geometrical phase transitions. (Bottom panels) θ'_G vs T at $\theta_f = \frac{3\pi}{4}$ (left) and θ'_G vs θ_f at $T = 0.6\omega_0$ (right). In both two cases, θ'_G exhibits π -jumps.

the parallel-transport condition, as shown in the bottom panel of Fig. 3. This can be understood by noting that in the non-geometric phase, the second term on the right-hand-side of Eq. (31) is always continuous and vanishes during parallel transport. The discontinuity can only arise from the first term, which appears in both cases with and without the parallel-transport condition. At fixed temperature $T = 0.6\omega_0$ but with varying end points labeled by θ_f , θ'_G also experiences a π -jump at about $\theta_f \approx 2.05$ rad, as indicated by the right panel in the bottom of Fig. 4. Therefore, the IGP and its non-adiabatic generalization of the CSS offer interesting predictions for future experimental investigations.

IV. GEOMETRICAL PHASES OF SSS

A. Uhlmann Phase

For the SSS shown in Eq. (5), the parameter space is one-dimensional. Therefore, we need to determine the value of Θ to define a cyclic process for density matrices, which is essential for generating the Uhlmann phase. The density matrix of a system in thermal equilibrium governed by $H(\Theta)$ show in Eq. (9) is given by $\rho(\Theta) = \frac{1}{Z}e^{-\beta H(\Theta)}$ with $Z = \text{Tr}(e^{-\beta H(\Theta)})$. By examining Eq. (6), we observe that the quadratic term of J_x

appears in the exponent, making it difficult to derive a general expression for the SSS. Therefore, for a concise illustration of the geometrical phases of the SSS, we will focus our studies on a fixed value of j . Since the behavior of the IGP for a two-level system ($j = \frac{1}{2}$) is relatively simple [67], we will begin with $j = 1$ for our analysis.

For the particular case of the $j = 1$ SSS, the corresponding angular momentum operators are

$$J_x = \begin{pmatrix} 0 & \frac{1}{\sqrt{2}} & 0 \\ \frac{1}{\sqrt{2}} & 0 & \frac{1}{\sqrt{2}} \\ 0 & \frac{1}{\sqrt{2}} & 0 \end{pmatrix}, J_y = \begin{pmatrix} 0 & \frac{i}{\sqrt{2}} & 0 \\ -\frac{i}{\sqrt{2}} & 0 & \frac{i}{\sqrt{2}} \\ 0 & -\frac{i}{\sqrt{2}} & 0 \end{pmatrix},$$

$$J_z = \begin{pmatrix} -1 & 0 & 0 \\ 0 & 0 & 0 \\ 0 & 0 & 1 \end{pmatrix}. \quad (32)$$

From Eq. (8), we have

$$S(\Theta) = \begin{pmatrix} \frac{1}{2} + \frac{1}{2}e^{-\frac{i\Theta}{2}} & 0 & -\frac{1}{2} + \frac{1}{2}e^{-\frac{i\Theta}{2}} \\ 0 & e^{-\frac{i\Theta}{2}} & 0 \\ -\frac{1}{2} + \frac{1}{2}e^{-\frac{i\Theta}{2}} & 0 & \frac{1}{2} + \frac{1}{2}e^{-\frac{i\Theta}{2}} \end{pmatrix}. \quad (33)$$

A straightforward calculation shows that when $\Theta = 4\pi$, $S(4\pi) = \mathbf{1}_{3 \times 3}$, which leads to $\rho(4\pi) = \rho(0)$ and gives a cyclic process. The 4π periodicity also contrasts the $j = 1$ SSS from an ordinary spin-1 state.

According to Eq. (12), the Uhlmann connection of the $j = 1$ SSS is

$$A_U = - \sum_{n \neq m} \chi_{nm} S |jn\rangle \langle jn| S^\dagger dS |jm\rangle \langle jm| S^\dagger$$

$$= \sum_{n \neq m} \chi S |jn\rangle \langle jn| \frac{i(J_+^2 + J_-^2)}{8} |jm\rangle \langle jm| S^\dagger d\Theta$$

$$= \frac{i\chi}{4} [J_x^2 - S J_y^2 S^\dagger] d\Theta, \quad (34)$$

where $\chi_{nm} = \frac{e^{-\beta m\omega_0} + e^{-\beta n\omega_0} - 2e^{-\frac{\beta(m+n)\omega_0}{2}}}{e^{-\beta m\omega_0} + e^{-\beta n\omega_0}}$, and $\chi \equiv \chi_{n,n+2} = \chi_{n+2,n} = \frac{(e^{\frac{\beta\omega_0}{2}} - e^{-\frac{\beta\omega_0}{2}})^2}{e^{\beta\omega_0} + e^{-\beta\omega_0}}$. In the last line, we have included the vanishing $n = m$ and $n = m - 1$ terms. It is in general challenging to find a nontrivial evolution path along which A_U is proportional to a constant matrix. The difficulty thus hinders the discovery of an analytical expression of the Uhlmann phase.

Nevertheless, numerical results can be obtained by using the Trotter-Suzuki approximation [68, 69] to tackle the path-ordered expression. Our findings are presented in Figure 5, where θ_U is plotted as a function of T on semi-log scale. Unlike the Uhlmann phase of the CSS, the Uhlmann phase of the SSS exhibits no discontinuities as the temperature varies, indicating the absence of a temperature-induced topological phase transition. The results show that at finite temperature, the initial and final purifications no longer remain parallel, but the “angle” between them changes continuously with temperature without any abrupt transition from “parallel”

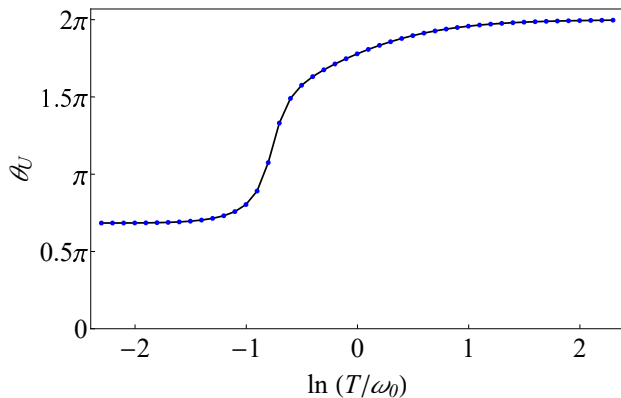


Figure 5. Uhlmann phase θ_U as a function of temperature T on semi-log scale. The smooth curve indicates the absence of a transition in this case.

to “antiparallel” as seen previously in the CSS. In the infinite temperature limit, $\theta_U = 2\pi \equiv 0 \pmod{2\pi}$ again. This is reasonable since $\lim_{T \rightarrow +\infty} \rho$ is proportional to the identity matrix, and the associated horizontal lift shrinks to a single point, resulting in $\lim_{T \rightarrow +\infty} \theta_U = 0 \pmod{2\pi}$ [24].

B. The interferometric geometric phase

To study the IGP of the SSS, we consider the unitary evolution

$$\rho(\Theta(t)) = \frac{1}{Z} e^{-\beta H(\Theta(t))} = S(\Theta(t)) \rho(\Theta(0)) S^\dagger(\Theta(t)), \quad (35)$$

where $\rho(\Theta(0)) = \rho(0) = \frac{1}{Z} e^{-\beta H}$. To ensure that S satisfies the parallel-transport condition (15), it is required that

$$\begin{aligned} 0 &= \text{Tr} \left[\rho(0) S^\dagger \dot{S} \right] \\ &= \sum_{m=-j}^j \langle jm | \frac{e^{-\beta\omega_0 J_z}}{Z} \frac{2J_- J_+ + 2J_z}{8} | jm \rangle \\ &= \sum_{m=-j}^j \frac{e^{-m\beta\omega_0}}{Z} \frac{j^2 + j - m^2}{4}. \end{aligned} \quad (36)$$

However, this condition cannot be satisfied at finite temperatures in general, so the IGP in its original form is not guaranteed. Therefore, the SSS provides an explicit example where a compatible evolution for generating the IGP is missing. This is in contrast to the Uhlmann phase based on the underlying Uhlmann bundle, which makes it possible to find the parallel transport on the geometric structure through the construction of the Uhlmann connection.

Nevertheless, one can still obtain the non-adiabatic IGP based on Eq. (19) accumulated during an arbitrary

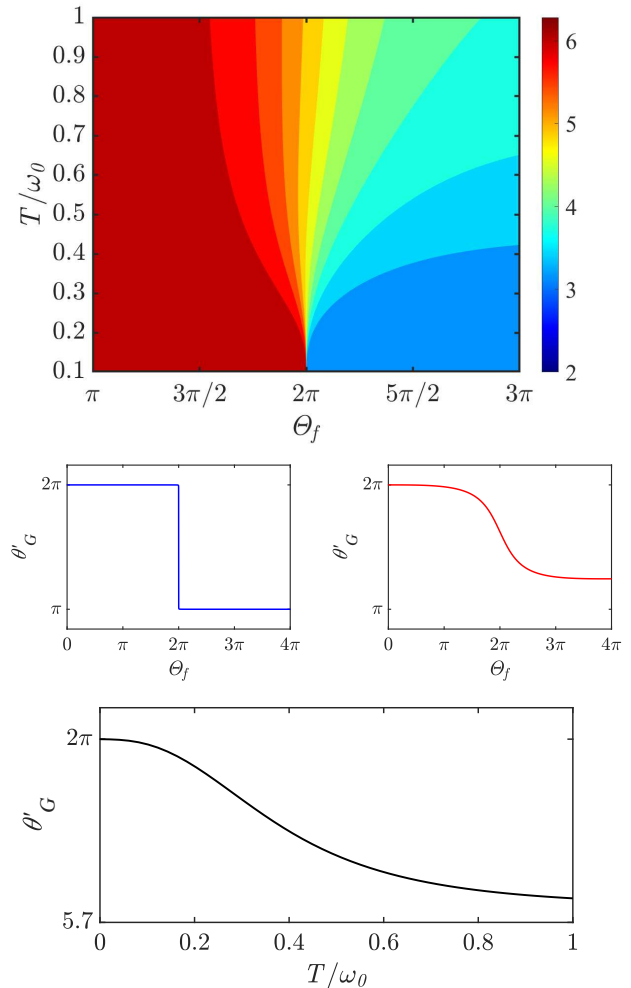


Figure 6. (Top panel) Contour plot of the non-adiabatic IGP θ'_G as a function of temperature T and the squeezing parameter Θ_f . (Middle panels) θ'_G vs Θ_f at $T = 0.0\omega_0$ (left) and $1.0\omega_0$ (right). (Bottom panel) θ'_G vs T for $\Theta_f = 5.4$.

evolution beyond the parallel-transport condition (15). To fairly compare with the results of the Uhlmann phase of the SSS, in the following we choose $j = 1$ for the non-adiabatic IGP as well. The total phase of the $j = 1$ SSS is given by

$$\begin{aligned} \theta_T(t) &= \arg \text{Tr}[\rho(0) S(\Theta(t))] \\ &= \arg \left[\left(\frac{1}{2} + \frac{1}{2} e^{-\frac{i\Theta(t)}{2}} \right) (e^{-\beta\omega_0} + e^{\beta\omega_0}) + e^{-\frac{i\Theta(t)}{2}} \right], \end{aligned} \quad (37)$$

and the non-geometric phase is

$$\begin{aligned} \theta_{\text{NG}}(t) &= -i \int_0^t \text{Tr}[\rho(0) S^\dagger(t') \dot{S}(t')] dt' \\ &= -\frac{2 + e^{-\beta\omega_0} + e^{\beta\omega_0}}{1 + e^{-\beta\omega_0} + e^{\beta\omega_0}} \frac{\Theta(t)}{4}. \end{aligned} \quad (38)$$

The non-adiabatic IGP is then obtained by $\theta'_G(t) = \theta_T(t) - \theta_{\text{NG}}(t)$. Since the evolution in this case is not

necessarily periodic, θ_G also depends on the final (instantaneous) time t .

In the top panel of Figure 6, the non-adiabatic IGP θ'_G is plotted as a function of temperature T and the squeezing parameter $\Theta_f \equiv \Theta(t_{\text{final}})$. Similar to the Uhlmann phase of the $j = 1$ SSS, there is no temperature-induced geometric phase transition here. We show the behavior of θ'_G as a function of T for $\Theta_f = 5.4$ in the bottom panel, in which θ'_G continuously decreases with T . At finite temperatures, we find that θ'_G also continuously varies with Θ_f without any discontinuities.

However, in the zero-temperature limit, $\theta_T = \arg[1 + e^{-\frac{i\Theta_f}{2}}]$ while θ_{NG} is always a continuous function of β and Θ_f . Therefore, as Θ_f crosses 2π , the midpoint of the parameter range $[0, 4\pi]$, the value of θ'_G experiences a π -jump (from $\frac{\pi}{2}$ to $-\frac{\pi}{2}$ or vice versa), indicating a geometric phase transition. We show this behavior of θ'_G in the middle-left panel of Figure 6. For comparison, we also plot θ'_G vs Θ_f at $T = 1.0\omega_0$ in the middle-right panel to contrast the smoothing of the curve at finite temperature. For the $j = 1$ SSS, therefore, finite-temperature jumps of the two types of mixed-state geometric phases are absent.

V. IMPLICATIONS

Since the CSS and SSS have been realized in condensed matter or atomic, molecular, and optical systems [53, 54, 70–72], experimental generation and measurement of the mixed-state geometric phases may become feasible in the future. However, imposing the parallel-transport condition for the IGP or Uhlmann phase requires precise controls of the systems and the ancilla representing the environment, which can be challenging in laboratories. Nevertheless, the non-adiabatic IGP relaxes the constraint and becomes a prominent candidate for demonstrating interesting geometric effects of CSS and SSS at finite temperatures. We caution that the non-adiabatic IGP is buried in the total phase, and a systematic removal of the non-geometric contribution according to Eq. (19) is required to obtain the genuine geometric contribution.

On the other hand, the rapid development of quantum computers opens possibilities of simulating complex quantum systems. By using an ancilla qubit acting as the environment and coupling it to a system qubit, Ref. [73] shows that the Uhlmann phase of a spin-1/2 system can be simulated on a quantum computer by using two engineered Hamiltonians to respectively evolve the system and ancilla simultaneously. Since a spin- j object may be decomposed as a collection of $2j$ spin-1/2 objects, one may use $2j$ qubits as a system of a spin- j system coupled to an ancilla system of $2j$ qubits to realize the CSS or SSS coupled to the environment. It then follows a series of technical challenges to construct suitable engineered Hamiltonians for the system and ancilla in order to generate the corresponding IGP or Uhlmann phase when the corresponding parallel-transport condition is

imposed during the evolution. After the targeted geometric phase is generated on a quantum computer, one may follow Ref. [73] to couple additional measurement qubits to the composite system and perform state tomography to extract the phase accumulated during the constrained evolution.

VI. CONCLUSION

We have derived the Uhlmann phase and the IGP along with its non-adiabatic generalization for the CSS and SSS. Selected examples are fully solved to demonstrate interesting properties of those mixed-state geometric phases. The Uhlmann phase is well-defined for both CSS and SSS due to its rigorous mathematical structure, but there may or many not be topological phase transitions manifested by discrete jumps of the Uhlmann phase as temperature varies. In contrast, the parallel-transport condition for the IGP does not have a general solution for the SSS although the IGP of the CSS exhibits discrete jumps. The non-adiabatic IGP forgoes the constraint and exhibits discrete jumps in the geometric part of the accumulated phase for the CSS. However, no finite-temperature jump is found in the non-adiabatic IGP for the $j = 1$ SSS. Our formalisms provide the foundation for future theoretical and experimental investigations of mixed-state topological properties of quantum spin systems.

ACKNOWLEDGEMENTS

H.G. was supported by the Innovation Program for Quantum Science and Technology (Grant No. 2021ZD0301904) and the National Natural Science Foundation of China (Grant No. 12074064). X.Y.H. was supported by the Jiangsu Funding Program for Excellent Postdoctoral Talent (Grant No. 2023ZB611). C.C.C. was supported by the National Science Foundation under Grant No. PHY-2310656.

Appendix A: Correspondence between Uhlmann phase and Berry phase of CSS as $T \rightarrow 0$

To evaluate the Uhlmann phase of the CSS, we introduce $g(t) = \mathcal{P}e^{-\int_0^t J_{0,\gamma} A_U(t') dt'}$, which is an operator depending on the evolution curve γ . Since $\gamma(\tau) = \gamma(0)$, $g(\tau)$ is in fact the Uhlmann holonomy. The operator $g(t)$ satisfies the differential equation

$$\frac{dg(t)}{dt} = \frac{\chi}{1 + |\zeta|^2} D(\zeta(t))(J_+ \dot{\zeta} - J_- \dot{\bar{\zeta}}) D^\dagger(\zeta(t)) g(t) \quad (\text{A1})$$

subject to the initial condition $g(0) = 1$. To solve this equation, we define $g'(t) = D^\dagger(\zeta(t))g(t)$. By taking the

complex conjugation of both sides of Eq. (23), we get

$$\dot{D}^\dagger D = \frac{1}{1+|\zeta|^2} \left[J_- \dot{\zeta} - J_+ \dot{\bar{\zeta}} + J_z \left(\bar{\zeta} \dot{\zeta} - \zeta \dot{\bar{\zeta}} \right) \right]. \quad (\text{A2})$$

Using Eqs. (A1) and (A2), we have

$$\begin{aligned} \frac{dg'(t)}{dt} &= \dot{D}^\dagger D g'(t) + \frac{\chi}{1+|\zeta|^2} \left(J_+ \dot{\zeta} - J_- \dot{\bar{\zeta}} \right) g'(t) \\ &= \frac{1}{1+|\zeta|^2} \left[-\eta \left(J_+ \dot{\zeta} - J_- \dot{\bar{\zeta}} \right) + J_z \left(\bar{\zeta} \dot{\zeta} - \zeta \dot{\bar{\zeta}} \right) \right] g'(t), \end{aligned}$$

where $\eta = \text{sech} \frac{\beta\omega_0}{2}$. Solving this equation, we obtain

$$g(\tau) = D(\zeta(\tau)) \mathcal{P}e^{\frac{\oint_\gamma [-\eta(J_+ d\zeta - J_- d\bar{\zeta}) + J_z(\bar{\zeta} d\zeta - \zeta d\bar{\zeta})]}{1+|\zeta|^2}} D^\dagger(\zeta(0)). \quad (\text{A3})$$

Therefore, the Uhlmann phase of the CSS is

$$\begin{aligned} \theta_U &= \arg \text{Tr} [\rho(\zeta(0)) g(\tau)] \\ &= \arg \text{Tr} \left[\rho(0) \mathcal{P}e^{\frac{\oint_\gamma [-\eta(J_+ d\zeta - J_- d\bar{\zeta}) + J_z(\bar{\zeta} d\zeta - \zeta d\bar{\zeta})]}{1+|\zeta|^2}} \right], \end{aligned} \quad (\text{A4})$$

where $\rho(0) = \frac{1}{Z} e^{-\beta\omega_0 J_z}$. As $T \rightarrow 0$, $\lim_{\beta \rightarrow \infty} \eta = \lim_{\beta \rightarrow \infty} \text{sech} \frac{\beta\omega_0}{2} = 0$, and $\rho(0) \approx |j, -j\rangle\langle j, -j|$, then

$$\begin{aligned} \lim_{T \rightarrow 0} \theta_U &= \arg \langle j, -j | \mathcal{P}e^{\frac{1}{1+|\zeta|^2} \oint_\gamma J_z (\bar{\zeta} d\zeta - \zeta d\bar{\zeta})} | j, -j \rangle \\ &= i \frac{j}{1+|\zeta|^2} \oint_\gamma (\bar{\zeta} d\zeta - \zeta d\bar{\zeta}), \end{aligned} \quad (\text{A5})$$

where $J_z |j, -j\rangle = -j |j, -j\rangle$ has been applied. This result precisely reduces to the Berry phase of the ground state $|j, -j\rangle$ [56]. More specifically, when $j = \frac{3}{2}$ and $\theta = \frac{\pi}{2}$, $|\zeta| = 1$ and thus $\theta_U = i \frac{3}{4} \oint_\gamma (-2i \tan^2 \frac{\theta}{2}) d\phi = 3\pi \equiv \pi \pmod{2\pi}$, which confirms the result shown in Fig. 1 as $T \rightarrow 0$.

-
- [1] A. Bohm, A. Mostafazadeh, H. Koizumi, Q. Niu, and J. Zwanziger, *The Geometric Phase in Quantum Systems* (Springer-Verlag, Heidelberg, Germany, 2003).
- [2] D. Chruscinski and A. Jamiolkowski, *Geometric Phases in Classical and Quantum Mechanics* (Birkhauser, Basel, Switzerland, 2004).
- [3] D. J. Thouless, M. Kohmoto, M. P. Nightingale, and M. den Nijs, *Phys. Rev. Lett.* **49**, 405 (1982).
- [4] F. D. M. Haldane, *Phys. Rev. Lett.* **61**, 2015 (1988).
- [5] M. Z. Hasan and C. L. Kane, Colloquium: Topological insulators, *Rev. Mod. Phys.* **82**, 3045 (2010).
- [6] X.-L. Qi and S.-C. Zhang, Topological insulators and superconductors, *Rev. Mod. Phys.* **83**, 1057 (2011).
- [7] C. L. Kane and E. J. Mele, *Phys. Rev. Lett.* **95**, 226801 (2005).
- [8] C. L. Kane and E. J. Mele, *Phys. Rev. Lett.* **95**, 146802 (2005).
- [9] C. K. Chiu, J. C. Y. Teo, A. P. Schnyder, and S. Ryu, Classification of topological quantum matter with symmetries, *Rev. Mod. Phys.* **88**, 035005 (2016).
- [10] B. A. Bernevig and T. L. Hughes, *Topological Insulators and Topological Superconductors* (Princeton, NJ, 2013).
- [11] B. A. Bernevig and S.-C. Zhang, *Phys. Rev. Lett.* **96**, 106802 (2006).
- [12] J. E. Moore and L. Balents, *Phys. Rev. B* **75**, 121306(R) (2007).
- [13] L. Fu, C. L. Kane, and E. J. Mele, *Phys. Rev. Lett.* **98**, 106803 (2007).
- [14] A. Bohm, A. Mostafazadeh, H. Koizumi, Q. Niu, and J. Zwanziger, *The geometric phase in quantum systems* (Springer, Berlin, Germany, 2003).
- [15] D. Vanderbilt, *Berry phases in electronic structure theory: electric polarization, orbital magnetization and topological insulators* (Cambridge University Press, 2018).
- [16] E. Cohen, H. Larocque, F. Bouchard, F. Nejdastari, Y. Gefen, and E. Karimi, Geometric phase from aharonov-bohm to pancharatnam-berry and beyond, *Nature Reviews Physics* **1**, 437 (2019).
- [17] A. Uhlmann, Parallel transport and "quantum holonomy" along density operators, *Rep. Math. Phys.* **24**, 229 (1986).
- [18] A. Uhlmann, On berry phases along mixtures of states, *Ann. Phys. (Berlin)* **501**, 63 (1989).
- [19] A. Uhlmann, The metric of bundles and the geometric phase, in *Groups and Related Topics: Proceedings of the First Max Born Symposium* edited by R. Gielera, J. Lukierski, and Z. Popowicz (Springer Netherlands, Dordrecht, 1992) pp. 267–274.
- [20] A. Uhlmann, A gauge field governing parallel transport along mixed states, *Letters in Mathematical Physics* **21**, 229 (1991).
- [21] X. Wang, X.-Y. Hou, Z. Zhou, H. Guo, and C.-C. Chien, Uhlmann phase of coherent states and the Uhlmann-Berry correspondence, *SciPost Phys. Core* **6**, 024 (2023).
- [22] J. C. Budich and S. Diehl, Topology of density matrices, *Phys. Rev. B* **91**, 165140 (2015).
- [23] O. Viyuela, A. Rivas, and M. A. Martin-Delgado, Uhlmann phase as a topological measure for one-dimensional fermion systems, *Phys. Rev. Lett.* **112**, 130401 (2014).
- [24] X.-Y. Hou, H. Guo, and C.-C. Chien, Finite-temperature topological phase transitions of spin- j systems in uhlmann processes: General formalism and experimental protocols, *Phys. Rev. A* **104**, 023303 (2021).
- [25] D. Morachis Galindo, F. Rojas, and J. A. Maytorena, Topological uhlmann phase transitions for a spin- j parti-

- cle in a magnetic field, *Phys. Rev. A* **103**, 042221 (2021).
- [26] J.-C. Tang, X.-Y. Hou, Z. Zhou, H. Guo, and C.-C. Chien, Uhlmann quench and geometric dynamic quantum phase transition of mixed states, *Phys. Rev. B* **110**, 134319 (2024).
- [27] E. Sjöqvist, A. K. Pati, A. Ekert, J. S. Anandan, M. Ericsson, D. K. L. Oi, and V. Vedral, Geometric phases for mixed states in interferometry, *Phys. Rev. Lett.* **85**, 2845 (2000).
- [28] M. Ericsson, E. Sjöqvist, J. Brännlund, D. K. L. Oi, and A. K. Pati, Generalization of the geometric phase to completely positive maps, *Phys. Rev. A* **67**, 020101 (2003).
- [29] A. Carollo, I. Fuentes-Guridi, M. F. Santos, and V. Vedral, Geometric phase in open systems, *Phys. Rev. Lett.* **90**, 160402 (2003).
- [30] J. G. P. de Faria, A. F. R. de Toledo Piza, and M. C. Nemes, Phases of quantum states in completely positive non-unitary evolution, *EPL* **62**, 782 (2003).
- [31] D. M. Tong, E. Sjöqvist, L. C. Kwek, and C. H. Oh, Kinematic approach to the mixed state geometric phase in nonunitary evolution, *Phys. Rev. Lett.* **93**, 080405 (2004).
- [32] L. C. Kwek, D. M. Tong, J. L. Chen, J. F. Du, K. W. Choo, R. Ravishankar, D. Kaszlikowski, and C. H. Oh, Geometric phase for mixed states, *Laser Physics* **16**, 398–401 (2006).
- [33] M. Ericsson, D. Achilles, J. T. Barreiro, D. Branning, N. A. Peters, and P. G. Kwiat, Measurement of geometric phase for mixed states using single photon interferometry, *Phys. Rev. Lett.* **94**, 050401 (2005).
- [34] J. Du, P. Zou, M. Shi, L. C. Kwek, J.-W. Pan, C. H. Oh, A. Ekert, D. K. L. Oi, and M. Ericsson, Observation of geometric phases for mixed states using nmr interferometry, *Phys. Rev. Lett.* **91**, 100403 (2003).
- [35] A. Ghosh and A. Kumar, Experimental measurement of mixed state geometric phase by quantum interferometry using nmr, *Physics Letters A* **349**, 27–36 (2006).
- [36] J. Klepp, S. Sponar, S. Filipp, M. Lettner, G. Badurek, and Y. Hasegawa, Observation of non-additive mixed-state phases with polarized neutrons, *Phys. Rev. Lett.* **101**, 150404 (2008).
- [37] X.-Y. Hou, X. Wang, Z. Zhou, H. Guo, and C.-C. Chien, Geometric phases of mixed quantum states: A comparative study of interferometric and uhlmann phases, *Phys. Rev. B* **107**, 165415 (2023).
- [38] O. Andersson, I. Bengtsson, M. Ericsson, and E. Sjöqvist, Geometric phases for mixed states of the kitaev chain, *Phil. Trans. R. Soc. A* **374**, 20150231 (2016).
- [39] X.-Y. Hou, Q.-C. Gao, H. Guo, Y. He, T. Liu, and C. C. Chien, Ubiquity of zeros of the loschmidt amplitude for mixed states in different physical processes and its implication, *Phys. Rev. B* **102**, 104305 (2020).
- [40] J. J. Sakurai and J. J. Napolitano, *Modern quantum mechanics*, 2nd ed. (Pearson, London, UK, 2010).
- [41] K. Huang, *Statistical Mechanics*, 2nd ed. (Wiley, Hoboken, NJ, 1991).
- [42] S. Bandyopadhyay and M. Cahay, *Introduction to Spintronics*, 2nd ed. (CRC Press, Boca Raton, FL, 2015).
- [43] A. Auerbach, *Interacting Electrons and Quantum Magnetism* (Springer-Verlag, Heidelberg, Germany, 1994).
- [44] C. M. Caves, Quantum-mechanical noise in an interferometer, *Phys. Rev. D* **23**, 1693 (1981).
- [45] V. Giovannetti, S. Lloyd, and L. Maccone, Quantum-enhanced measurements: Beating the standard quantum limit, *Science* **306**, 1330 (2004).
- [46] D. J. Wineland, J. J. Bollinger, W. M. Itano, F. L. Moore, and D. J. Heinzen, Spin squeezing and reduced quantum noise in spectroscopy, *Phys. Rev. A* **46**, R6797 (1992).
- [47] L. Pezze and A. Smerzi, Quantum theory of phase estimation, in *Atom interferometry* (IOS Press, 2014) pp. 691–741.
- [48] M. Kitagawa and M. Ueda, Squeezed spin states, *Phys. Rev. A* **47**, 5138 (1993).
- [49] J. Ma, X. Wang, C. Sun, and F. Nori, Quantum spin squeezing, *Physics Reports* **509**, 89 (2011).
- [50] M. Block, B. Ye, B. Roberts, S. Chern, W. Wu, Z. Wang, L. Pollet, E. J. Davis, B. I. Halperin, and N. Y. Yao, Scalable spin squeezing from finite-temperature easy-plane magnetism, *Nature Physics* **20**, 1575 (2024).
- [51] D. J. Wineland, J. J. Bollinger, W. M. Itano, and D. J. Heinzen, Squeezed atomic states and projection noise in spectroscopy, *Phys. Rev. A* **50**, 67 (1994).
- [52] W. J. Eckner, N. Darkwah Oppong, A. Cao, A. W. Young, W. R. Milner, J. M. Robinson, J. Ye, and A. M. Kaufman, Realizing spin squeezing with rydberg interactions in an optical clock, *Nature* **621**, 734 (2023).
- [53] J. Estève, C. Gross, A. Weller, S. Giovanazzi, and M. K. Oberthaler, Squeezing and entanglement in a bose-einstein condensate, *Nature* **455**, 1216–1219 (2008).
- [54] C. Gross, T. Zibold, E. Nicklas, J. Estève, and M. K. Oberthaler, Nonlinear atom interferometer surpasses classical precision limit, *Nature* **464**, 1165–1169 (2010).
- [55] M. F. Riedel, P. Böhi, Y. Li, T. W. Hänsch, A. Sinatra, and P. Treutlein, Atom-chip-based generation of entanglement for quantum metrology, *Nature* **464**, 1170–1173 (2010).
- [56] S. Chaturvedi, M. S. Sriram, and V. Srinivasan, Berry’s phase for coherent states, *Phys. A: Math. Gen.* **20**, L1071 (1987).
- [57] C. Chryssomalakos, E. Guzmán-González, and E. Serrano-Ensástiga, Geometry of spin coherent states, *Journal of Physics A: Mathematical and Theoretical* **51**, 165202 (2018).
- [58] A. M. Perelomov, *Generalized Coherent States and their Applications* (Springer Science and Business Media LLC, 1986).
- [59] J. M. Radcliffe, Some properties of coherent spin states, *J. Phys. A: Math. Theor.* **4**, 313 (1971).
- [60] F. Xue, Y.-x. Liu, C. P. Sun, and F. Nori, Two-mode squeezed states and entangled states of two mechanical resonators, *Phys. Rev. B* **76**, 064305 (2007).
- [61] H. Guo, X.-Y. Hou, Y. He, and C.-C. Chien, Dynamic process and uhlmann process: Incompatibility and dynamic phase of mixed quantum states, *Phys. Rev. B* **101**, 104310 (2020).
- [62] A. Uhlmann, Geometric phases and related structures, *Rep. Math. Phys.* **36**, 461 (1995).
- [63] J. Zhang, T. H. Kyaw, S. Filipp, L.-C. Kwek, E. Sjöqvist, and D. Tong, Geometric and holonomic quantum computation, *Physics Reports* **1027**, 1 (2023), geometric and holonomic quantum computation.
- [64] N. Mukunda and R. Simon, Quantum kinematic approach to the geometric phase. i. general formalism, *Ann. Phys.* **228**, 205 (1993).
- [65] S. Mohammadi Almas and G. Najarbashi, Geometric phase for mixed squeezed-coherent states (2024), arXiv:2410.15482.
- [66] X.-Y. Hou, H. Guo, and C. C. Chien, Finite-temperature topological phase transitions of spin- j systems in

- uhlmann processes: General formalism and experimental protocols, *Phys. Rev. A* **104**, 023303 (2021).
- [67] O. Andersson, I. Bengtsson, M. Ericsson, and E. Sjöqvist, Geometric phases for mixed states of the kitaev chain, *Philosophical Transactions of the Royal Society A: Mathematical, Physical, and Engineering Sciences* **374**, 20150231 (2016).
- [68] H. F. Trotter, On the product of semi-groups of operators, *Proc. Amer. Math. Soc.* **10**, 545–551 (1959).
- [69] M. Suzuki, Generalized trotter’s formula and systematic approximants, *Commun. Math. Phys.* **51**, 183–190 (1976).
- [70] L.-G. Huang, F. Chen, X. Li, Y. Li, R. Lü, and Y.-C. Liu, Dynamic synthesis of heisenberg-limited spin squeezing, *npj Quantum Information* **7**, 10.1038/s41534-021-00505-z (2021).
- [71] T. Byrnes, Multipartite spin coherent states and spinor states, *Phys. Rev. A* **109**, 022438 (2024).
- [72] M. A. Kasevich, Quantum phase magnification, *Science* **352**, 1552 (2016).
- [73] O. Viyuela, A. Rivas, S. Gasparinetti, A. Wallraff, S. Filipp, and M. A. Martin-Delgado, A measurement protocol for the topological uhlmann phase, *npj Quant. Inf.* **4**, 10 (2018).